Energy Reports 10 (2023) 2260–2276

Contents lists available at ScienceDirect

Energy Reports

journal homepage: www.elsevier.com/locate/egyr

3E assessment of a solar-driven reverse osmosis plant for seawater desalination in a small island of the Mediterranean Sea

S. Guarino *, P. Catrini, A. Buscemi, V. Lo Brano, A. Piacentino

Department of Engineering, University of Palermo, Viale delle Scienze, 90128, Palermo, Italy

ARTICLE INFO

Article history:
Received 15 March 2023
Received in revised form 2 August 2023
Accepted 4 September 2023
Available online xxxx

Keywords:
Solar desalination
Dish-Stirling system
Reverse osmosis
Seawater desalination
Energy assessment
Levelized Cost Of Water

ABSTRACT

Water scarcity in many regions of the world and global demographic growth make the desalination of seawater and/or brackish an effective solution to meet the growing demand for fresh water. Nowadays, reverse osmosis has the largest share of the global installed desalination capacity. The impelling need to reduce greenhouse gas emissions has been pushing the search for sustainable technologies to produce the electricity needed to power reverse osmosis plants. Among solar technologies, little attention has been paid to the possibility of powering reverse osmosis with electricity from the dish-Stirling solar concentrator. To fill this knowledge gap, this paper assesses the energy-saving potential of a reverse osmosis plant coupled with a cogenerative dish-Stirling concentrator on a small island in the Mediterranean Sea. A model of the integrated systems was developed based on data measured on a real dish-Stirling concentrator. Moreover, the variation of the energy consumption of the reverse osmosis plant with the temperature of the feedwater solution was also accounted for. Hourly simulations showed that almost 36% of the annual water demand could be covered by driving the plant using electricity from the concentrator, and the solar fraction of the electricity consumed by the reverse osmosis plant accounted for 48%. Finally, economic and environmental analyses revealed that the levelized cost of water of €1.08 per cubic meter of fresh water, consistent with the literature, and the system could avoid emitting 34.16 tons of carbon dioxide equivalent emissions per year.

1. Introduction

It is widely recognized that desalination technologies play a key role in addressing water scarcity in both arid regions and densely populated areas in the world. However, recent climate change will exacerbate water scarcity issues, making desalination technologies essential not only in arid regions but also in those that currently rely on fresh water from natural sources (Unfried et al., 2022). According to recent statistics (Eke et al., 2020), the global installed desalination capacity amounts to about 100 million m^3/day. More specifically, reverse osmosis (RO) accounts for about 69%, multi-stage flash (MSF) for 17%, and multi-effect distillation (MED) for only 7%.

RO is a process in which solvent molecules are forced to move from the more concentrated solution to the less concentrated solution through a semi-permeable membrane (Greenlee et al., 2009). For this purpose, a pressure greater than the osmotic pressure is applied to the more concentrated solution. For desalination purposes, the membrane allows the solute (brine) contained in the treated seawater or brackish water to be separated from the pure solvent, thus obtaining permeate water. Therefore, desalination technology based on RO essentially requires electrical energy or mechanical energy to drive pumps that increase the pressure of the feed water to be treated before it can pass through the semi-permeable membrane. The specific energy consumption (SEC) of the RO process typically ranges between 1.5 and 4 kWh/m^3 (Alsarayreh et al., 2020; Kim et al., 2019; Xevgenos et al., 2016). Worth noting that, the RO share on global installed capacity steeply increased after 1960–1970, thanks to the technological improvement in membranes manufacturing, which allowed to overcome issues related to membrane fouling (Shenvi et al., 2015).

During the decades, several studies were published with the scope of reducing the SEC of RO systems (Zapata-Sierra et al., 2021). For instance, some authors investigated alternative flow arrangements (Sayyad et al., 2022) or optimized the operation while accounting for the daily variation of fresh water demand and seawater temperature (Sassi and Mujtaba, 2013). Others evaluated the benefits achievable by hybridizing RO with other desalination technologies such as MED or electrodialysis (Almulla et al., 2005; Feria-Díaz et al., 2021). Other authors investigated the possibility to boost the performance of the RO plants by using waste heat or thermal energy from renewable energy sources (RES) to preheat the feedwater (Kelley and Dubowsky, 2013; Shalaby et al., 2022). In this respect, as proven by Karabelas et al.

* Corresponding author.
E-mail address: stefania.guarino@unipa.it (S. Guarino).

https://doi.org/10.1016/j.egyr.2023.09.053

(2018), the control of the temperature of the feedwater could help to reduce the SEC value compared to cases where the temperature is not monitored.

Considering the large share of RO plants in the worldwide desalination capacity, it is interesting to investigate if RES may be alternatively used to supply these systems (Nassrullah et al., 2020). Indeed, the achievable benefits are twofold. First, it would increase the sustainability of the produced fresh water, thanks to the avoided carbon dioxide (CO_2) emissions which would be emitted if the electricity was produced by fossil-fueled power plants. Secondly, it could solve the water scarcity in places not easily reachable by the power grid. Research studies focused on the coupling of RES with RO systems were published during these years (Okampo and Nwulu, 2021). RESs such as geothermal (Loutatidou and Arafat, 2015), ocean (Leijon et al., 2018), wind (Gökçek and Gökçek, 2016), solar energy (Shalaby, 2017), and their combinations (Lee et al., 2018) were considered as a solution to drive desalination plants. However, the high unit cost of the fresh water produced from RES-RO plants has represented a barrier to their widespread. In this respect, in Al-Karaghouli and Kazmerski (2013) it was found that wind energy could be highly suitable to power desalination plants, with several projects already implemented, featuring capacities ranging from 50 to 2000 m^3/day. The associated costs vary between 6.6 and 9.0 US$/$m^3$ for seawater desalination and between 1.95 and 5.2 US$/$m^3$ for brackish water desalination. On the other hand, in Al-Karaghouli and Kazmerski (2013) it was found that RO systems integrated with solar photovoltaic setups are mainly used in small-scale installations with capacities below 100 m^3/day. In this case, the production costs for these systems typically range between 11.7 and 15.6 US$/$m^3$ for seawater desalination and between 6.5 and 9.1 US$/$m^3$ for brackish water desalination (Al-Karaghouli and Kazmerski, 2013). To meet the water demand in a cost-effective, efficient, and environmentally friendly manner, it is essential to effectively combine RES and desalination technologies (Ghazi et al., 2022).

Focusing on solar-powered RO plants, in a review paper from Shalaby et al. (2022), it was pointed out that photovoltaic (PV) is the most used RES. Almost all RO desalination plants powered by solar thermal energy rely on Organic Rankine cycle systems (Li et al., 2013). However, according to Fiorenza et al. (2003), the integration of RO with PV systems seems to be cheaper than solar-driven thermal desalination plants. Abdelgaied et al. proposed an innovative system based on a photovoltaic–thermal solar collector (PVT) coupled with a solar dish concentrator to drive an RO desalination unit. More specifically, the PVT modules were used to power the RO unit while the thermal energy recovered from the PV modules and the solar dish concentrator was used to pre-heat the feedwater to be desalted. Thanks to the preheating step, which increased membrane permeability and reduced fluid friction losses across the membrane, an average 35% reduction in specific power consumption was achieved in the case of brackish water desalination, and a 20% reduction was found for seawater (Abdelgaied et al., 2022).

The integration of RO plants with concentrating solar power systems (CSP) is an attractive option for those regions characterized by both severe water shortage and high solar irradiation (e.g., the Middle East and North Africa region) (Aboelmaaref et al., 2020).

Al-Dafaie et al. investigated the possibility to use the heat recovered from a dish-Stirling concentrator to supply a membrane distillation unit (Al-Dafaie et al., 2016). Aboelmaaref et al. estimated that fresh water produced by an RO plant powered by a parabolic trough is more economical than the one obtained by a parabolic trough-MED-TVC plant (Aboelmaaref et al., 2020). Palenzuela et al. presented a simulation tool for assessing power generation and fresh water production from solar-driven desalination plants in different locations. Among all proposed configurations, the integration of a RO desalination plant with a CSP system was found to be the best combination in southern Europe, with maximum water and electricity production (Palenzuela et al., 2020). In Casimiro et al. (2017), the physical performance of a water and electricity co-generation system consisting of a CSP plant using a parabolic trough system and a seawater RO unit located in Trapani (southern Italy) was examined. The CSP-RO system was compared to a CSP plant-powered MED unit at the same location. The results indicated that the CSP-RO system can generate approximately 46% of the total output of the full-scale plant in Trapani while providing around 14% more water and 20% more electricity compared to the CSP-MED system. Conversely, few studies focused on the coupling of RO plants with a dish-Stirling concentrator. Geng et al. analyzed an RO desalination system powered by using the mechanical energy produced by a solar dish-Stirling concentrator. The authors found that water productivity is highly sensitive with the temperature of the absorber (Geng et al., 2021).

The previous literature review points out that there is a large interest in research for using solar energy for desalination purposes. In addition, the limited number of published papers on RO plants coupled with a dish-Stirling concentrator suggests that an unexplored potential of this technology in this field may exist. In this respect, to the authors' knowledge, the possibility to operate the dish-Stirling concentrator in a cogenerative mode, when supplying RO systems, has not been investigated yet. Indeed, twofold benefits could arise from the exploitation of thermal energy recovered from the concentrator to pre-heat the feed water supplied to RO plant: (i) an increase in the membrane permeability which leads to greater fresh water production (Abdelgaied et al., 2022), and (ii) an increase of the energy output of the solar concentrator (i.e., the recovery of waste heat from the cold side of the Stirling engine) which is usefully exploited during the operation of the concentrator (Guarino et al., 2021).

In this framework, the present study aims at investigating the possibility of powering an RO desalination system for seawater treatment (here follow indicated as SWRO) through a cogenerative dish-Stirling system. More specifically, an energy, assessment of the layout of the proposed integrated plant was carried out, considering that all or part of the electric energy required to produce desalinated water is covered with renewable energy from the solar source. For this purpose, a dynamic simulation model was developed on *Transient System Simulation* (TRNSYS) environment of the integrated plant layout including the dish-Stirling system and an RO system. The model was developed by using real data collected from a dish-Stirling system installed at the University of Palermo. Meantime, the simulation relied on performance maps of the RO plant which accounted for the effect of seawater temperature on the SEC. As a case study, it was assumed that the integrated desalination plant is located on a small Mediterranean island, such as Lampedusa (Sicily, Italy). In addition, economic and environmental analyses were carried out, evaluating the levelized cost of water (LCOW) produced by the examined solar-driven SWRO plant and the amount of CO_2 equivalent emissions avoided thanks to the production of electricity from solar sources.

The paper was structured as follows. In the second section, a schematic representation of the solar-driven desalination plant is provided, along with an explanation of the energy model utilized for the energy analysis, and the methodologies employed to conduct the economic and environmental analyses. The third section outlines the case study, which includes a description of the reference dish-Stirling system, the RO system under consideration, a brief overview of the chosen location for the desalination

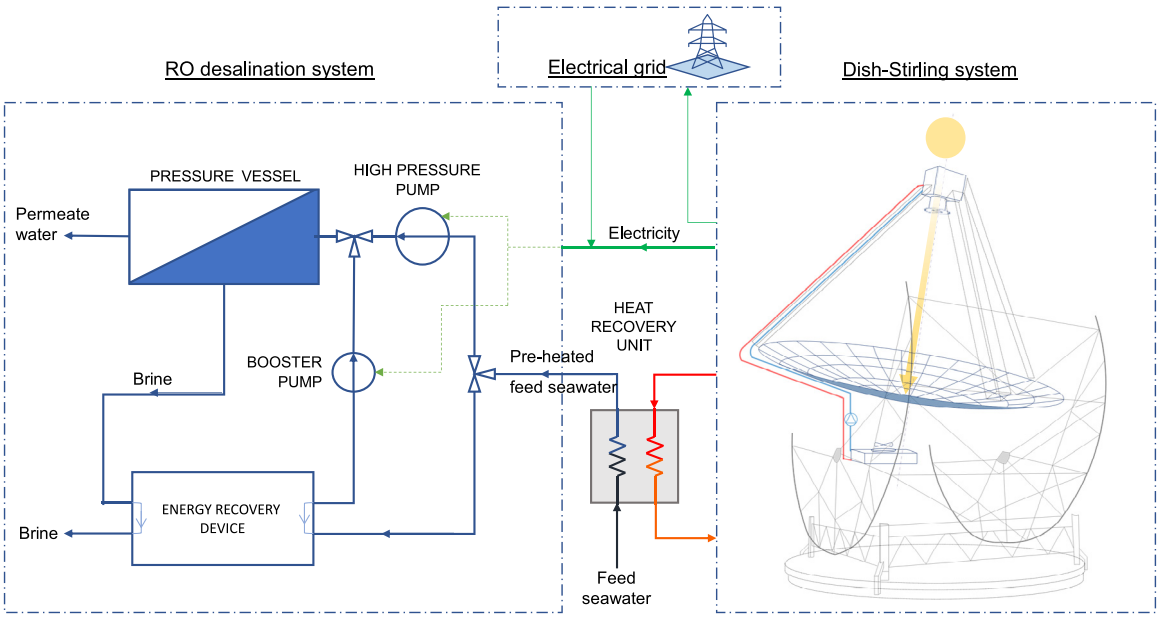

Fig. 1. A schematic representation of the solar-SWRO desalination plant layout.

plant, and the preliminary assumptions made for the economic analysis. In the fourth section, the results obtained from the study are presented in detail. Finally, the fifth section contains the concluding remarks drawn from the study's findings.

2. Material and methods

This section describes the examined plant layout to produce fresh water by using an SWRO desalination system driven by a dish-Stirling system. Then, the mathematical models of each subsystem are shown together with the implementation in TRNSYS.

2.1. Schematic description of a solar-powered desalination system

Fig. 1 shows a schematic layout of the examined solar-powered plant for the production of fresh water, which includes: a RO desalination system, a dish-Stirling solar concentrator, and a heat recovery unit.

The dish-Stirling system is a point-focusing CSP technology that enables the conversion of solar energy into electricity by achieving high conversion efficiency. Specifically, the direct solar irradiation collected by the paraboloidal reflector is concentrated onto a receiver that transfers the high-temperature thermal energy to a working fluid. Once the working fluid has achieved the required pressure and temperature operating conditions, it is elaborated in the Stirling engine according to the four thermodynamic transformations of the homonymous cycle. The mechanical energy generated by the engine is finally converted into electricity by an electric generator. The high efficiency of the Stirling engine is ensured by the cooling of its cold side by a system that dissipates the waste of low-temperature heat in the environment.

As shown in Fig. 1, the operation of the proposed integrated desalination plant involves both the electricity and thermal energy produced by the dish-Stirling system: the renewable electricity produced from solar power is used to power the pumps of the seawater circuit, and the low-temperature thermal energy, otherwise dissipated in the environment, is recovered by a thermal recovery unit to pre-heat the seawater before to be processed in the RO system. It was also assumed that, when no electricity is available from the solar concentrator, the SWRO plant uses electricity supplied from the grid; on the other hand, when the solar concentrator produces electricity and this is not required by the SWRO plant or exceeds its demand, it was assumed that any surplus electricity produced is fed into the grid.

2.2. Energy modeling of the solar-driven SWRO plant

This subsection describes and defines the mathematical model developed to simulate the operation of the proposed integrated system and, thus, to evaluate its energy performance.

2.2.1. Energy modeling of the dish-Stirling system

According to the mathematical model developed by some of the authors of this study (Buscemi A. et al.), it is possible to state that there is a linear correlation between the electrical outpower of the dish-Stirling system and the incident direct solar irradiance (Buscemi et al., 2020).

Dish-Stirling solar concentrators convert direct solar irradiation into electricity and the solar input power collected by the paraboloidal reflector $\left(\dot{Q}_{solar}\right)$ can be defined by Eq. (1):

$$\dot{Q}_{solar} = I_b \cdot A_{dish} \tag{1}$$

where, I_b is the solar beam irradiance, expressed in [W/m^2], and A_{dish} indicates the net effective area of the reflector.

Then, as shown in Eq. (2), the solar power focused on the receiver $\left(\dot{Q}_{r,in}\right)$ can be evaluated by reducing the solar input power of the reflector by a fraction accounting for the total optical losses.

$$\dot{Q}_{r,in} = \eta_o \cdot \eta_{cle} \cdot \dot{Q}_{solar} \tag{2}$$

In the latter equation: η_o is the optical efficiency of the concentrator which is obtained as a product of the reflectivity of clean mirrors (ρ), the intercept factor (γ), and the absorbance of the receiver cavity (α); and η_{cle} is the cleanliness index of the mirrors.

Due to the difference in temperature between the receiver surface and the environment, the receiver is affected by convective and radiative thermal losses. Thus, the thermal power output from the receiver $\left(\dot{Q}_{r,out}\right)$ can be calculated as follows:

$$\dot{Q}_{r,out} = A_r \cdot \left\{ h_r \cdot \left(T_r^{ave} - T_{air}\right) + \sigma \cdot \varepsilon \cdot \left[\left(T_r^{ave} + 273.15\right)^4 - \left(T_{sky} + 273.15\right)^4 \right] \right\} \tag{3}$$

where:

- A_r is the aperture area of the receiver.
- h_r is the free convective heat-transfer coefficient at the receiver surface.
- T_r^{ave} is the average value of the receiver surface temperature.
- T_{air} is the external air temperature.
- σ is the Stefan–Boltzmann constant.
- ε is the emissivity of the receiver surface.
- T_{sky} is the effective sky temperature, i.e. the equivalent black-body temperature of the sky calculated as (Ahmadi, 2012; Bădescu, 1991; Kongtragool and Wongwises, 2005):

$$T_{sky} = 0.0552 \cdot (T_{air} + 273.15)^{1.5} - 273.15$$

Then, the high-temperature thermal power delivered to the Stirling engine $\left(\dot{Q}_{S,in}\right)$ corresponds to the thermal input power of the receiver reduced by the convective and radiative thermal losses towards the environment $\left(\dot{Q}_{r,out}\right)$, as defined by Eq. (4):

$$\dot{Q}_{S,in} = \dot{Q}_{r,in} - \dot{Q}_{r,out} \tag{4}$$

As it was experimentally validated in the study conducted by the same authors of this study (Buscemi et al., 2020), the mechanical power produced by the Stirling engine $\left(\dot{W}_S\right)$ can be evaluated by a linear relation as a function of the thermal input power of the engine as follows:

$$\dot{W}_S = \left(a_1 \cdot \dot{Q}_{S,in} - a_2\right) \cdot R_T \tag{5}$$

where, a_1 and a_2 are two fitting parameters, and R_T is a temperature correction factor which is the ratio between the air temperature and the reference air temperature (set at 25 °C), both expressed in Kelvin.

Therefore, the low-temperature thermal power discharged from the cold side of the Stirling engine $\left(\dot{Q}_{S,out}\right)$ can be defined as a difference between the thermal input power and the mechanical power at the crankshaft as follows:

$$\dot{Q}_{S,out} = \dot{Q}_{S,in} - \dot{W}_S \tag{6}$$

While on the hot side of the engine, the receiver supplies high-temperature thermal power, on the cold side, the thermal power defined by Eq. (6) is dissipated into the environment through a dry cooler. Otherwise, it could be recovered to pre-heat the seawater feeding the RO system as proposed in this work.

Finally, it is possible to deduce the net electrical output power of the dish-Stirling system from Eq. (7) below:

$$\dot{E}_n = \eta_e \cdot \dot{W}_S - \dot{E}_p \tag{7}$$

where, η_e is the conversion efficiency of the electric generator and $\dot{E}_p$ is the electric power absorbed by the parasitic components, such as the tracking solar system and the cooling system.

As can be seen from Eq. (1), the solar power input to the concentrator depends on the value of direct solar irradiance and the size of the reflecting surface constituting the paraboloidal collector. In this respect, the solar concentrator is typically sized to operate for solar beam radiation values within a range whose minimum and maximum limit values represent operational limits for the conversion power unit: for I_b values below the lower operating limit of the system, the solar power input to the concentrator is insufficient to allow the fluid evolving in the Stirling engine to reach the nominal temperature and pressure conditions; on the contrary, for I_b values above the upper operating limit of the system, the thermal power that would be delivered to the Stirling engine would be higher than the maximum power it would be able to handle, causing its failure.

When choosing a location, it is essential to verify compatibility in terms of the weather and climate characteristics of the site for the installation of the solar concentrator. Then, it is also worth investigating whether the system sizing can be optimized. In this respect, in a recent paper published by the authors Buscemi et al. (2021), a methodology for the optimal sizing of the dish-Stirling concentrator was proposed. More specifically, from the analysis of characteristic solar data for a specific installation location and by reconstructing the hourly frequency distribution of I_b, it may emerge that the most frequent I_b value in a year does not coincide with the I_b value for which the dish-Stirling system was designed. A particular case would be if the most frequent I_b value is lower than the solar beam irradiance value that identifies the maximum operability limit for which the solar concentrator was sized, and this last value occurs for only a few hours in a year. This means that the dish-Stirling system will operate for very few hours per year at its maximum potential. In this case, to maximize the energy production of the system, it would be possible to increase the reflecting surface of the collector until the maximum solar power that can be processed is obtained precisely at the most frequent I_b value typical of the selected location while keeping the power conversion unit unchanged. For the few hours of the year when the solar beam irradiance value exceeds the most frequent I_b value for the selected location, which has become the new upper limit of system operability, it may be possible to activate a specific air cooler for the receiver to dissipate the excess thermal power concentrated.

2.2.2. Specific energy consumption of the RO system

In the case SWRO plant, it is first necessary to pre-treat the feed water to remove large particles and solids that would otherwise foul the surfaces of the RO membranes. Then, as shown in Fig. 1, the pressure level of the feed seawater is raised to above osmotic pressure using a High-Pressure Pump (HPP), to proceed with the desalination process by crossing the membranes of the various modules constituting the pressure vessel. Finally, at the outlet of the pressure vessel, the permeate is treated before being supplied to the user and the brine is delivered to the Energy Recovery Device (ERD) before being disposed of. The most advanced RO systems use an ERD to recover residual pressure energy from the brine flow reducing the electricity consumption required by the high-pressure pump. In this way, part of the feed seawater flow will reach the setpoint pressure (at the pressure vessel inlet) by a booster pump (BP) bypassing the HPP (Amr Omar et al., 2022). To evaluate the energy performance of the plant, the SEC is used. This indicator is defined as the energy per volume unit required to produce the permeate water and it is usually measured in [kWh/m^3]. As it was stated in (Kim et al., 2019), the SEC of a RO desalination plant depends on several factors, such as the temperature and salinity conditions of the feed seawater, the quality of the fresh water to be obtained, and the efficiency of the RO system. Moreover, the efficiency of the HPP and booster pump, along with the one of ERD, affects the total SEC value (Karabelas et al., 2018; Koutsou et al., 2020).

Starting from the energy balance of the RO unit and assuming that the HPP and BP have the same efficiency, it is possible to deduce the following SEC expression (Karabelas et al., 2018; Koutsou et al., 2020):

$$SEC = \frac{W_{tot}}{\dot{V}_p} = \frac{1}{R} \cdot \left[\frac{P_f - P_p}{\eta}\right] + (1-\beta) \cdot \left[\frac{1-R}{R}\right] \cdot \left[\frac{P_p + \eta_E \cdot \Delta P - \eta_E \cdot P_f}{\eta}\right] \tag{8}$$

In the latter equation:

- W_{tot} is the total power required by the HPP and BP, expressed in [kW].
- $\dot{V}_p$ is the permeate water flow rate, expressed in [m^3/h].

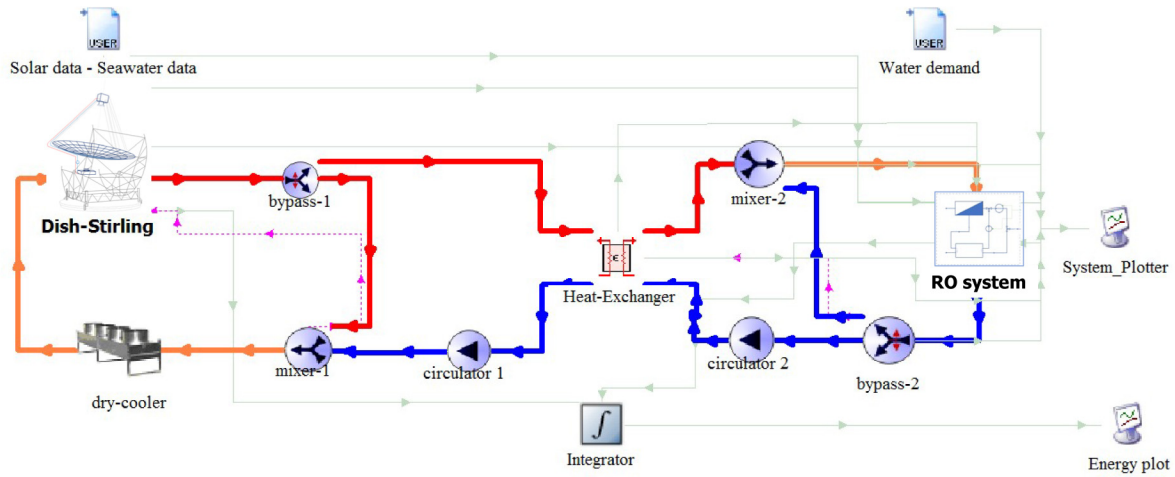

Fig. 2. TRNSYS layout for modeling the operation of the solar-powered SWRO desalination plant.

- R is the permeate recovery ratio, i.e., the ratio between the permeate flow rate and feed seawater flow rate.
- P_f and P_p are pressure levels of feed seawater and permeate, respectively, expressed in [bar].
- ΔP is the pressure difference across the RO unit, i.e., the difference in pressure between the feed seawater and brine.
- β is the leakage water flow rate fraction of the ERD.
- η_E is the efficiency of the ERD.
- η is the efficiency of the two pressure pumps in the circuit.

The salinity and temperature of the feed water are the factors that most influence the energy demand of the RO system. For the same temperature of the feed water, according to van't Hoff's equation (Ghaffour et al., 2014), a higher salinity of the seawater implies a higher osmotic pressure and, therefore, more energy required by the pumps to get the water to the operating pressure level. On the other hand, as the temperature increases, essentially both the water and salt permeability coefficient of the semi-permeable membrane increase. Under these conditions, the desalination process requires less pressure energy and, thus, less SEC will be achieved (Kim et al., 2019).

For seawater, a salinity of between 35000 and 40000 mg/l can be considered, and modern SWRO systems generally have an SEC lower than 2.5 kWh/m^3 (Ghaffour et al., 2014). Note that the energy consumption required for water pre-treatment should be included. This consumption typically ranges between 0.2 and 0.8 kWh/m^3 (Ghaffour et al., 2014).

2.2.3. Modeling the operation of the proposed solar-driven SWRO desalination plant

Fig. 2 shows the TRNSYS layout used to model the operation of the proposed plant scheme. On the left-hand side of the layout, there are placed the components (Types) modeling the dish-Stirling solar concentrator with its dry-cooler, whereas, on the right-hand side, those modeling the RO system. A Heat EXchanger (HEX) is placed between the two sides allowing the transfer of the heat rejected from the dish-Stirling to the circuit feeding the RO System with the seawater. The temperature of the fluid leaving the cooling circuit of the dish-Stirling is set at approximately 40 °C. The heat rejected by the dry-cooler of the dish-Stirling, however, changes as a function of the direct normal irradiance (DNI) variations and, therefore, depends on the partial-load functioning of the Stirling engine. Thus, both diverter and mixer valves ("bypass-1" and "mixer-1" in Fig. 2, respectively) were inserted into the hydraulic circuit to handle these variations in the heat to be rejected. In other words, the flow of hot water leaving the dry cooler and directed to the source side of the HEX is partly diverted ("bypass-1" in Fig. 2) and mixed ("mixer-1" in Fig. 2) with the cold water returning from the source side of the HEX, before entering the dry-cooler again. This approach permits the control of the water temperature at the dry-cooler inlet, which always works with a constant water flow rate.

On the right side of the plant layout, seawater enters the load side of the exchanger to be pre-heated with the heat transferred from the dish-Stirling cooling system, before being delivered to the RO system. Two valves were also inserted in this part of the hydraulic circuit: a diverter and a mixing valve ("bypass-2" and "mixer-2" in Fig. 2, respectively). These valves operate whenever the temperature exiting the load side of the HEX exceeds a value of 30 °C. Based on the results shown in (Koutsou et al., 2020) and here discussed in Section 3.2, this value was selected in order to obtain the minimum SEC, when seawater is used as feed solution. If this happens, part of the cold seawater flow is diverted, before entering the source side of the HEX ("bypass-2" in Fig. 2) and mixed ("mixer-2" in Fig. 2) with the cold water coming from the load side of the HEX before to be delivered to the RO system.

2.3. Economic analysis

The cost of producing desalinated water through reverse osmosis depends on various factors, such as the size of the plant, the technology used, the salinity of the feed water, the cost of electricity, and the cost of feed water. In general, reverse osmosis is considered one of the most efficient and cost-effective desalination technologies available, as it requires less energy compared to other commercially widespread technologies. However, the actual cost depends on the specific conditions of each plant (Elazhar et al., 2015).

On average, the cost of producing desalinated water through RO can range from about 0.5 to 2 €per cubic meter of water produced, depending on the specific conditions of the plant (Caldera et al., 2016). However, it is important to note that the cost can vary significantly depending on local conditions and the above-mentioned factors, so each case needs to be evaluated individually to determine the actual cost of producing desalinated water through reverse osmosis (Goosen et al., 2023). The sustainable commercialization of renewable energy technologies for solar desalination is a complex process that involves not only economic and environmental considerations but also local markets and the policies/regulations of various governments, which may either drive or pose a barrier to market development (Goosen et al., 2023).

The LCOW is an important economic metric for determining the competitiveness of a seawater desalination plant. The levelized cost of produced desalinated water represents the average cost of the water produced, including all the costs associated with the water production facility, such as capital expenditures, operating costs, maintenance costs, financing costs, and any other costs that may affect the production of water. The LCOW can be compared with the price of conventional water (from sources such as rivers, lakes, wells, etc.) and can be used to compare the cost of producing water from different sources or using different technologies. According to (Papapetrou et al., 2017), the LCOW can be obtained by using Eq. (9):

$$LCOW = \frac{I_0 + \sum_{t=1}^{N} \frac{C_t}{(1+i)^t}}{\sum_{t=1}^{N} \frac{M_{w,t}}{(1+i)^t}} \tag{9}$$

where, I_0 is the initial capital investment, C_t is the annual operation cost, $M_{w,t}$ is the total amount of desalinated water produced in year tth, the variable N represents the lifespan of the plant under consideration (expressed in years), and i is the discount rate.

In the case of the proposed solar-driven SWRO plant, determining the LCOW requires some considerations. This integrated plant uses both on-site electricity generated by the dish-Stirling solar concentrator and electricity drawn from the grid when the solar concentration system is not functioning. Additionally, it is necessary to consider that when the dish-Stirling system produces more electricity than the SWRO system requires, any surplus energy is sold to the national electrical grid. Therefore, in Eq. (9), the term I_0 was calculated as the sum of the capital investment cost for the SWRO plant $\left(I_0^{RO}\right)$ and that for the dish-Stirling facility $\left(I_0^{DS}\right)$.

The overall operational costs were calculated by considering operational costs for the SWRO plant and those for the dish-Stirling systems (respectively indicated as C_t^{RO} and C_t^{DS}). The former of these two terms was assessed by taking into account the maintenance costs of the desalination plant $\left(C_{M,t}^{RO}\right)$ and the costs related to the required portion of energy that was purchased from the national grid $\left(C_{energy,t}^{RO}\right)$. In addition, it was also considered the revenue resulting from the sale of surplus electricity produced by the solar concentrator (R_t). Under these considerations, the LCOW can be evaluated as follows:

$$LCOW = \frac{\left(I_0^{RO} + I_0^{DS}\right) + \sum_{t=1}^{n} \frac{C_t^{RO} + C_t^{DS} - R_t}{(1+i)^t}}{\sum_{t=1}^{n} \frac{M_{w,t}}{(1+i)^t}} \tag{10}$$

where:

$$C_t^{RO} = C_{M,t}^{RO} + C_{energy,t}^{RO} \tag{11}$$

As can be observed in Eq. (12), the cost term $C_{energy,t}^{RO}$ was evaluated by multiplying the annual energy demand of the SWRO $\left(E_t^{RO}\right)$ by the cost related to the purchased electricity $\left(c_{energy}\right)$ by the complement of the solar fraction (f_{sol}).

$$C_{energy,t}^{RO} = E_t^{RO} \cdot c_{energy} \cdot (1 - f_{sol}) \tag{12}$$

Finally, the revenue term R_t was evaluated as follows:

$$R_t = E_{exs,t}^{DS} \cdot p_{ex} \tag{13}$$

where, $E_{exs,t}^{DS}$ is the annual surplus of energy produced by the solar concentrator and exported to the grid at the selling price p_{ex}.

2.4. Environmental analysis

In this work, it was assumed that the energy produced by the solar field is mainly used to produce fresh water and, in the remaining part, to supply the national power grid. The amount of avoided CO_2 emissions was quantified by assuming that all the amount of energy had been produced from fossil fuels. It was assessed by multiplying the energy produced from solar sources by the median value of lifecycle greenhouse gas (GHG) emissions that are associated with the Italian energy production context.

Fig. 3. The dish-Stirling CSP plant installed at the university campus in Palermo (Italy).

The median values of greenhouse gas emissions over the lifecycle refer to the average amount of greenhouse gases (such as carbon dioxide, methane, and nitrous oxide) emitted throughout the entire life cycle of a product, process, or technology. The median value is often used to represent the central tendency of a set of data, and it provides a measure of typical greenhouse gas emissions that can be used for comparison between different products, processes, or technologies (Hondo, 2005). The corresponding values for technologies fueled by non-renewable sources reach 0.469, 0.84, and 1.001 $kgCO_{2e}$/kWh for natural gas, oil, and coal, respectively (Edenhofer et al., 2011). According to data and statistics published by the International Energy Agency (IEA), from the fossil fuel energy mix that characterizes Italy, it was possible to deduct the median value of lifecycle GHG emissions that amounts to 0.546 $kgCO_{2e}$/kWh (Guarino et al., 2022). Considering this median value of lifecycle GHG emissions (expressed in $kgCO_{2e}$/kWh), that is indicated as $\mu_{\substack{fuel \\ mix}}^{CO_2}$, and the annual production of electricity from solar energy $\left(E_r^{renew.}\right)$, it was then possible to determine the amount of avoided CO_2 emissions in terms of tons per year $\left(CO_2{}^{av}\right)$ by using the following equation:

$$CO_2{}^{av} = E_r{}^{renew.} \cdot \mu_{\substack{fuel \\ mix}}^{CO_2} \cdot 10^{-3} \tag{14}$$

3. Case study

3.1. The dish-Stirling reference plant

In this study, the dish-Stirling system that has been taken as a reference is the demonstration plant installed at the university campus in Palermo (southern Italy) (see Fig. 3). It has a net electric peak output power of 31.5 kW_e (when DNI is 960 W/m^2,

Table 1
Main technical characteristics of the dish-Stirling plant of Palermo and parameters of the related model.

Technical data	Value	Unit
Net effective area of the dish (A_{dish})	106	m^2
Aperture area of the receiver (A_r)	0.0314	m^2
Average parasitic electric consumption ($\dot{E}_p^{ave}$)	1600	W
Clean mirrors' optical efficiency (η_o)	0.85	–
Convective heat transfer coefficient of the receiver (h_r)	10	W/(m^2 K)
Emissivity of the receiver (ε)	0.88	–
Focal length	7.45	m
Geometric concentration ratio	3517	–
Max operating pressure of hydrogen	200	bar
Mirror cleanliness index (η_{cle})	0.85	–
Parameter a_1 in Equation (5)	0.475	–
Parameter a_2 in Equation (5)	3318.66	W
Reference temperature (T_0)	25	°C
Reflectivity of clean mirror (ρ)	0.95	–
Average temperature of the receiver (T_r^{ave})	720	°C

Table 2
Data referring to the RO system (Karabelas et al., 2018; Koutsou et al., 2020).

Data	Value	Unit
Salinity of seawater	40,000	ppm
Desalination capacity	300	m^3/day
Recovery ratio	0.5	–
No. of pressure vessel	1	–
Elements in each pressure vessel	7 (Spiral Wound Membrane)	–
Membrane area of module	37	m^2
Number of envelopes	15	–
Membrane sheet length	0.96	m
Membrane sheet width	1.285	m
Water membrane permeability (for seawater at T=25 °C)	1.23	[l/(m^2 h)]/bar
ΔP for friction losses per pressure vessel	136,1	kPa

the temperature of the air is 25 °C, and the mirrors are clean) and represents the state-of-the-art in parabolic dish technology with a solar-to-electric energy conversion efficiency of up to 32% (a record achieved in a similar plant installed by Ripasso Energy in the Republic of South Africa) (Coventry and Andraka, 2017).

This CSP plant has a high geometric concentration ratio of 3517 and a high conversion efficiency ensured by the good optical efficiency of the concentrator, the high precision of the biaxial tracking system, and the high-performance Stirling engine as it consists of four double-acting cylinders equipped with regenerators. Moreover, the used working fluid is hydrogen, which under the system's operating conditions has a low viscosity, minimizing fluid-dynamic friction losses (Lo Brano et al., 2022). The main technical characteristics of this plant are reported in Table 1.

3.2. The RO system

Unlike the modeling of the dish-Stirling system, which is based on operating data collected experimentally during the measurement campaign of a real existing plant, a black-box model is used to assess the energy required by the RO unit during its operation. This model is based on data found in the literature (Karabelas et al., 2018; Koutsou et al., 2020). Some data of the RO plant, such as membrane properties and other technical data, are summarized in Table 2. However, for more information, readers are invited to refer to (Karabelas et al., 2018; Koutsou et al., 2020).

As shown in Fig. 4, to consider the effect of the temperature of the feed water (T_f) on the total specific energy consumption of the RO unit, a second-order fitting function was derived from the data plotted in the following graph, by taking a fixed salinity value (Koutsou et al., 2020). More in detail, as shown in (Koutsou et al., 2020), the SEC curve plotted in Fig. 4 is a result of different counterbalancing effects. Indeed, although the increase in temperature of the feed seawater leads to a beneficial decrease in water viscosity (thus reducing the energy consumption of the pump), it involves a substantial increase in solution osmotic pressure (thus increasing the minimum energy required for the separation process). For this reason, a minimum SEC value is found.

Finally, worth noting that the feed water temperature may not be the same as the seawater temperature (T_{sea}) if, for example, a pre-heating unit is provided in the desalination system.

3.3. Details on the installation site

Lampedusa (35.519 N, 12.564 E) is a small island in the Italian archipelago of the Pelagie Islands in Sicily, with an area of 20.2 km ^{2} and approximately 5,800 inhabitants.

This island is not connected to the mainland electricity grid and uses electricity generated through a diesel-fueled thermoelectric power plant. On the other hand, the water demand is met by using seawater desalination plants. Lampedusa could be suitable to host a solar-driven desalination plant such as the one proposed because of its high level of solar radiation of about 2,107.9 kWh/m^2/year.

Fig. 5 shows the hourly direct normal irradiance and air temperature data which were extrapolated from the Typical Meteorological Year provided by the PVGIS-SARAH2 solar database, with reference to the decade between 2005 and 2016 (Pfeifroth et al., 2019). These data were used as input in the dish-Stirling model to assess the energy producibility of the solar system.

Furthermore, using the same solar data, the hourly frequency distribution of DNI was derived for frequency classes of 50 W/m^2, and the mean value of air temperature was obtained for each class (see Fig. 6). It can be noted that the most frequent DNI value for Lampedusa falls within the DNI range between 800 and 850 W/m^2, and the number of annual hours in which a DNI value higher than 950 W/m^2 is observed is less than 10. In cases like this, as also anticipated in Section 2.2.1, the reference dish-Stirling solar concentrator, which has been designed for a

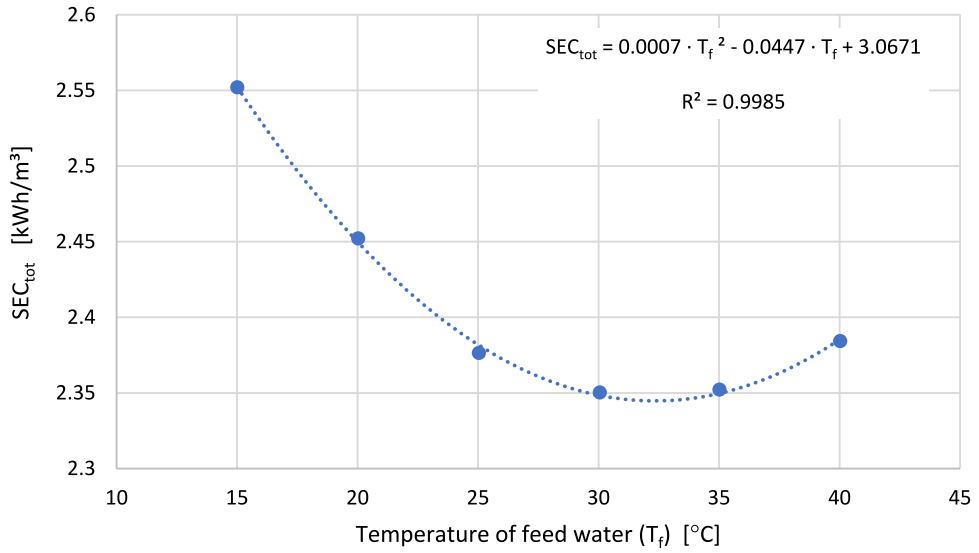

Fig. 4. The specific energy consumption as a function of the feed water temperature (T_f) (Koutsou et al., 2020).

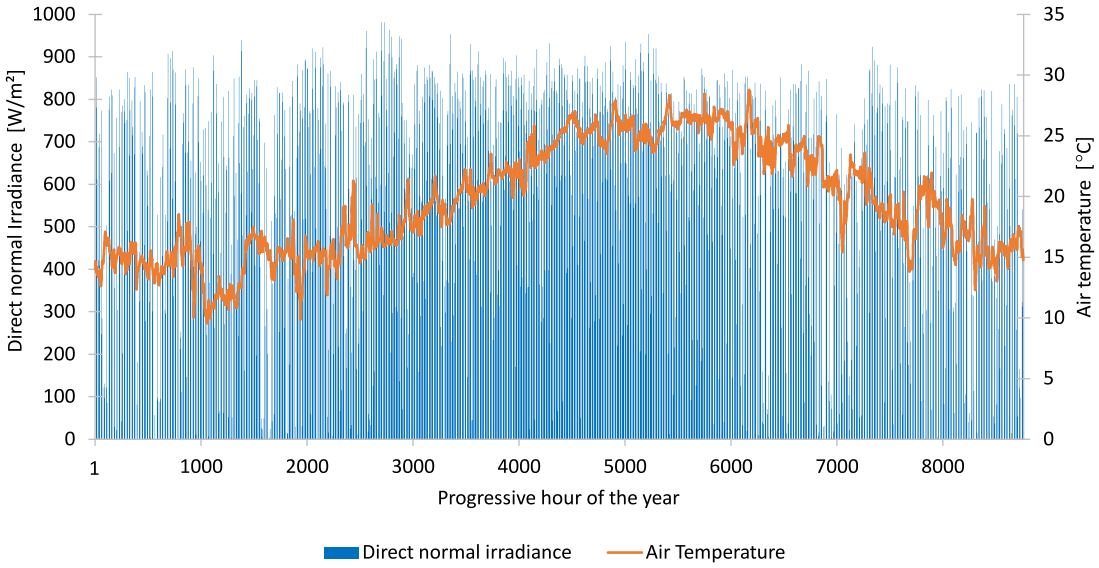

Fig. 5. Hourly direct normal irradiance and air temperature for the locality of Lampedusa.

maximum DNI value of 960 W/m^2, if installed in Lampedusa, will almost always operate at a power level below its maximum and therefore could be optimized to maximize its annual energy production.

To evaluate the specific energy consumption of the RO unit, the variable value of the seawater temperature was determined as a sinusoidal function of the progressive day of the year (see Fig. 7). This function, calibrated on the monthly average seawater temperature values for Lampedusa (Weather stats: forecast, statistics, analysis, 2022), is reported in Eq. (14) below.

$$T_{sea} = 20.6553 + 6.1699 \cdot \sin\left[3.72936 + \frac{2\pi n}{365}\right] \quad (15)$$

In this work, it was considered the water demand of a district of Lampedusa (about 600 people) is approximately 61,161 m^3/year. Fig. 8 shows the monthly aggregate water demand and the hourly average water demand for each month.

3.4. Assumptions for the economic analysis

As previously mentioned in Section 2.3, the LCOW values enable the comparison of different technologies for the production of desalted water. Table 3 provides the values of all input variables used to calculate the LCOW (see Eqs. (10) to (13)) for the proposed solar-driven seawater reverse osmosis plant.

Specifically, to evaluate the investment cost related to the desalination unit, literature data were used, and a capital expenditure (*capex*) of €3,914/(m^3 year) was considered for the investigated SWRO plant, which has a small desalination capacity of less than 1000 m^3 per day. This led to an investment cost (I_0^{RO}) of €239,378.00 (Caldera and Breyer, 2017). For the same plant, regarding the operating expenses (*opex*), it was assumed that they were equal to 5% of the capital expenditures (Caldera et al., 2016).

Unlike the assumed costs for the SWRO plant, the investment and operational costs assumed for the dish-Stirling plant consider

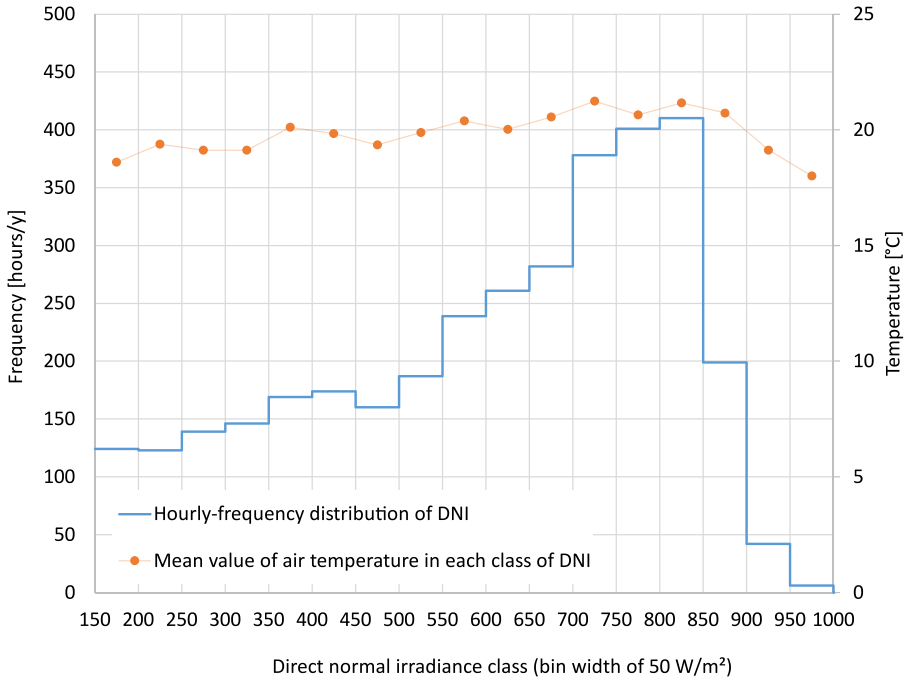

Fig. 6. Hourly-frequency distribution of DNI and mean values of air temperature for each class of DNI for Lampedusa.

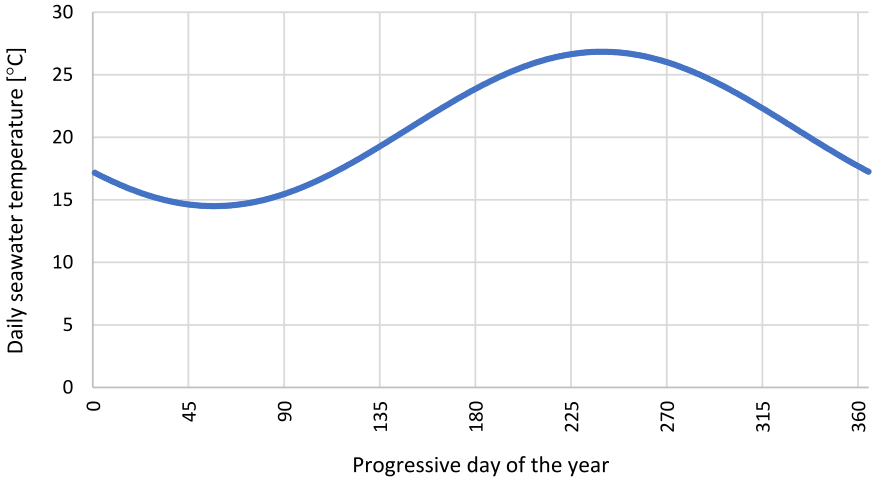

Fig. 7. The plot of the sinusoidal function of seawater temperature (T_{sea}) as a function of the progressive day of the year.

Table 3
Input variables of the LCOW metric.

LCOW input variables	Value	Unit
Seawater reverse osmosis plant		
Capital expenditure (*capex*) (Caldera and Breyer, 2017)	3.914	[€/(m^3 year)]
Operating expenses (*opex*) (Caldera et al., 2016)	0.195	[€/(m^3 year)]
Purchase cost of electricity from the grid (c_{energy})	0.223	[€/kWh]
Solar fraction (f_{sol})	48	[%]
Annual energy demand (E_t^{RO})	110.32	[MWh/year]
Annual amount of produced fresh water ($M_{w,t}$)	61,161	[m^3/year]
Lifespan (N)	20	[years]
Discount rate (i) (Papapetrou et al., 2017)	8	[%]
Dish-Stirling solar concentrator		
Total investment cost (I_0^{DS})	172,028.00	[€]
Annual operating cost (C_t^{DS})	2,622.31	[€/year]
Annual exported energy surplus to the grid ($E_{exs,\,t}^{DS}$)	9.49	[MWh/year]
Selling price (p_{ex})	0.04	[€/kWh]

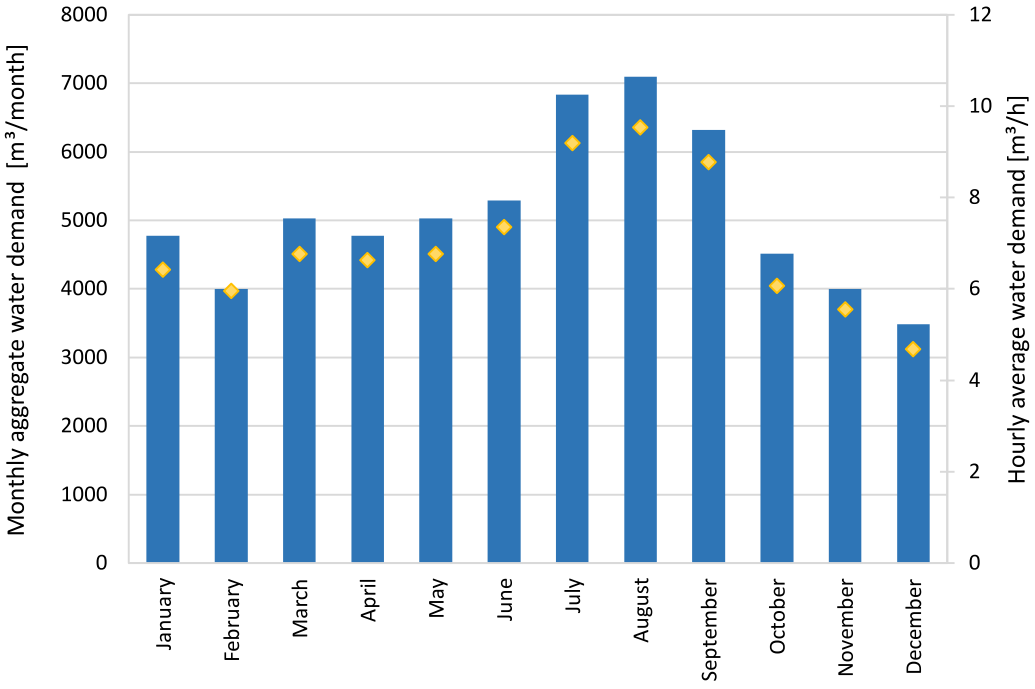

Fig. 8. Monthly aggregate water demand and the hourly average water demand for each month of Lampedusa.

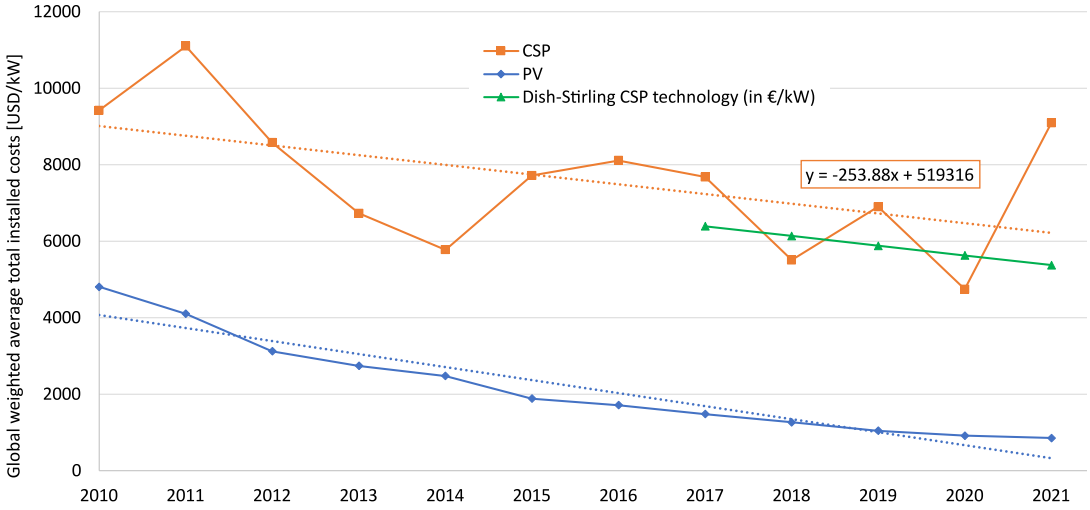

Fig. 9. Global weighted average installed costs of solar technologies.. (For interpretation of the references to color in this figure legend, the reader is referred to the web version of this article.)

the actual costs incurred for the installation of the prototype plant referred to in Section 3.1, which occurred in 2017. Starting from the total installed cost incurred in 2017, which was €6,391.4/kW, a cost reduction assumption over time was applied, taking into account the possible effect of increased installed capacity resulting from greater market diffusion. Parabolic dish technology is currently the least commercially mature among other CSP technologies. For this study, it was assumed that starting from 2017, the total installed costs of the parabolic dish concentrator technology were affected by the same negative trend that has been seen in the costs of other CSP technologies, namely parabolic troughs, central towers, and Fresnel reflectors, in accordance with data published by the International Renewable Energy Agency (IRENA) (see green line in Fig. 9).

Under these assumptions, capital expenditure of €5,375.88/kW (reduced by 16% compared to the actual costs incurred for the installation of the Palermo dish-Stirling system) and an annual cost for the maintenance and operation of the system of €2,622.31 per year were assumed. The same reduction trend was applied to these latter maintenance costs as to the total investment cost.

For the calculation of costs corresponding to the purchase of electricity from the grid (c_{energy}), a purchase cost of €0.223/kWh (see Table 3) was considered. This value was calculated as the mean of the annual average purchase cost of electricity (in Italy indicated as Prezzo Unico Nazionale – PUN) for the years 2021, 2022, and 2023. As shown in Fig. 10, a forecast was made for 2023, assuming that, given the values for the first quarter, the purchase price of electricity would continue to rise for the rest

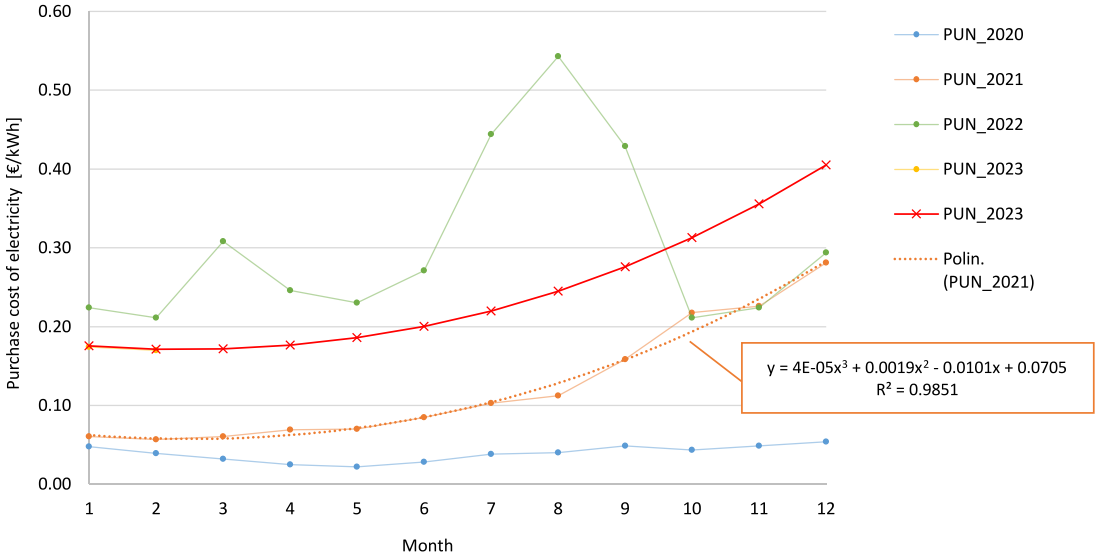

Fig. 10. The assumption for the forecast of the purchase price of electricity from the grid in 2023.

of the year with the same growth trend recorded for 2021. The trend in purchasing costs on the national grid for 2022 was not considered because, as can be seen from Fig. 17, it was extremely variable due to interruptions in gas supply through Ukraine that caused instability in the prices of gas and other fossil fuels in Western Europe and the consequent increase in electricity prices, since in Italy electricity is produced for about 50% from natural gas (IEA, 2023).

4. Results and discussion

This section presents the results obtained from the study conducted on fresh water production using the reverse osmosis desalination system integrated with a dish-Stirling solar concentrator, operating in a purely electric mode or cogeneration mode (when the waste heat from the Stirling engine is recovered to pre-heat the seawater feeding the desalination plant). In addition, results obtained from economic and environmental analyses for the same integrated system are also outlined.

4.1. The optimal dish-stirling system configuration for Lampedusa

As shown in Fig. 6, the peak of the hourly DNI frequency obtained for Lampedusa corresponds to an average DNI value of 825 W/m^2, while the reference dish-Stirling plant was designed for a maximum DNI value of 960 W/m^2. Therefore, as explained in Section 2.2.1, an optimization study was carried out to find a suitable geometric configuration of the solar concentrator for the solar characterization of Lampedusa. In other words, different configurations of the solar concentrator were explored, each with an increasingly reflective surface to lower the maximum operating limit of the Stirling engine to the most probable DNI value (i.e. the peak value of the hourly DNI frequency distribution) for Lampedusa. As shown in Fig. 11, this optimization objective was achieved for a reflective surface of the collector increased by 20% (127.2 m^2) compared to that of the reference system (106 m^2). This optimized dish-Stirling system configuration allows for an annual energy production of about 62.6 MWh, 25% more than the reference system configuration (∼50 MWh/y) in Lampedusa.

4.2. Results from annual simulations

Before showing data on annual water production and energy consumption of the integrated system, it is worth discussing some preliminary results which prove the capability of the proposed model in supporting the analysis of these systems. For instance, Fig. 12 shows the hourly production of fresh water from the solar-powered SWRO system. The thickening of the columns for the central hours of the year (as highlighted by the red box in Fig. 12) suggests a higher water production during the summer when the highest irradiation is available. A comparison between Figs. 12 and 8 reveals a temporal matching between the maximum water production from the solar source and the highest water demand.

Focusing on a clear sky summer day, Fig. 13 shows the following profiles: the total demand of the RO plant (light blue), the total energy production of the solar field (orange), the energy output from the solar field delivered to the RO plant (green), and the energy demand of the RO plant provided by the grid (purple). Note that the grid supplies the SWRO plant during the early morning and sunset (purple line) when the DNI values are lower than the cut-in value. Additionally, the light orange shaded area corresponds to the surplus energy produced by the solar field that is not consumed by the desalination plant and sold to the grid. This accounts for almost 7.4% of the total energy produced by the concentrator.

As previously mentioned, the model accounts for the variation of SEC value with the temperature of the feedwater (see Fig. 7). It is interesting to show the accuracy gained compared to a model which relies on a constant value of feedwater temperature.

Fig. 14 shows that the electricity consumption of the RO unit is overestimated by about 7 MWh per year if a constant value of the feedwater temperature is assumed. This quantity corresponds to about 11% of the annual net electricity produced by the dish-Stirling system. Indeed, as will be shown later (see Fig. 14), the annual electricity production of the examined solar concentrator is about 62.6 MWh.

As shown in Fig. 15, the annual cumulative electric energy production of the dish-Stirling system, operating in cogenerative mode, amounts to about 62.6 MWh. At the same time, the annual cumulative electricity required by the RO plant is 110.32 MWh and the annual amount of electricity exported to the grid is 9.49

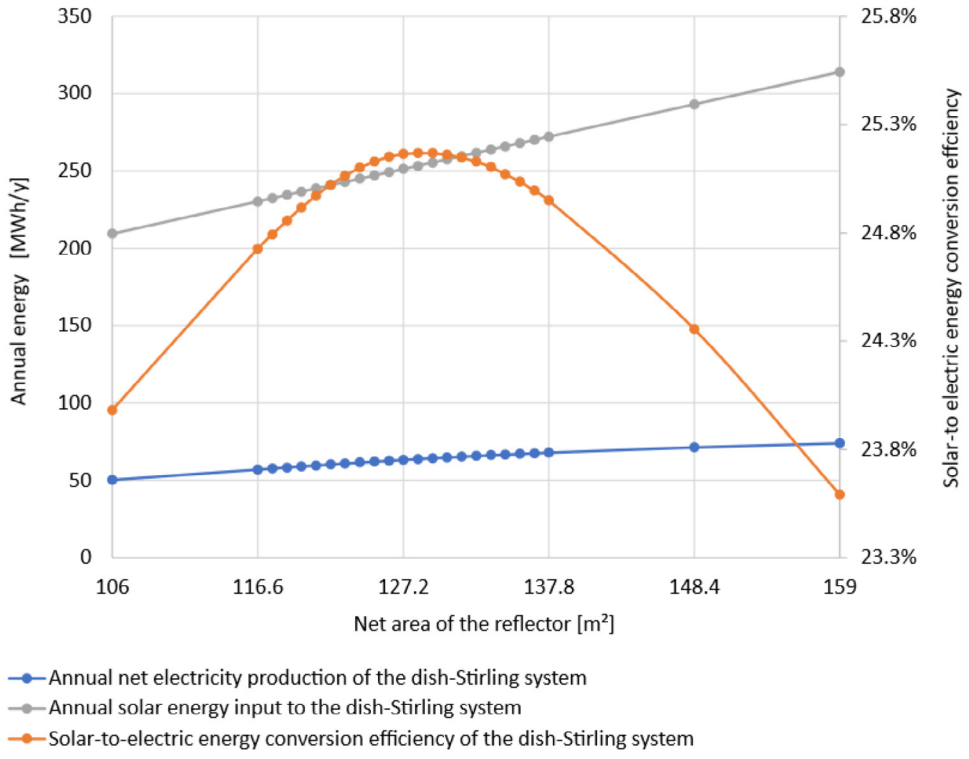

Fig. 11. Optimization of the dish-Stirling solar concentrator for Lampedusa.

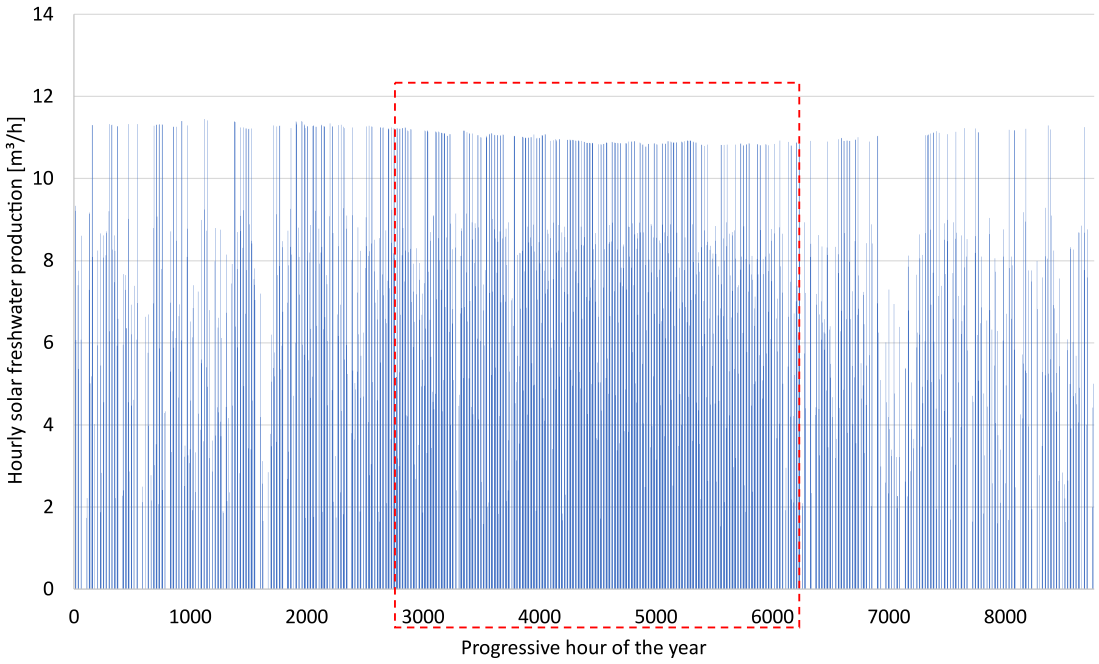

Fig. 12. Hourly fresh water production from the solar-powered SWRO system.

MWh. In percentage terms, it has been found that annually 85% of the electricity generated by the solar field would be used to cover part of the energy demand of the SWRO plant, while the remaining 15% would be sold to the grid. Therefore, a solar fraction of the SWRO plant of about 48% was achieved on an annual basis, with solar fraction referring to the fraction of energy demand covered by the solar source. The remaining 52% of the energy demand of the SWRO system would be provided by the grid.

Fig. 16 shows that the amount of fresh water produced by using electricity from the solar concentrator accounts for approximately 36% of the total water demand. The remaining fraction of the demand is covered by using electricity from the power grid.

Finally, the simulations were repeated to quantify the effect of the absence of feedwater preheating on the electricity required by the RO system. Fig. 17 shows the annual cumulative curves of the energy requirement of the RO unit in the presence and absence of heat recovery. It is possible to observe that the feedwater

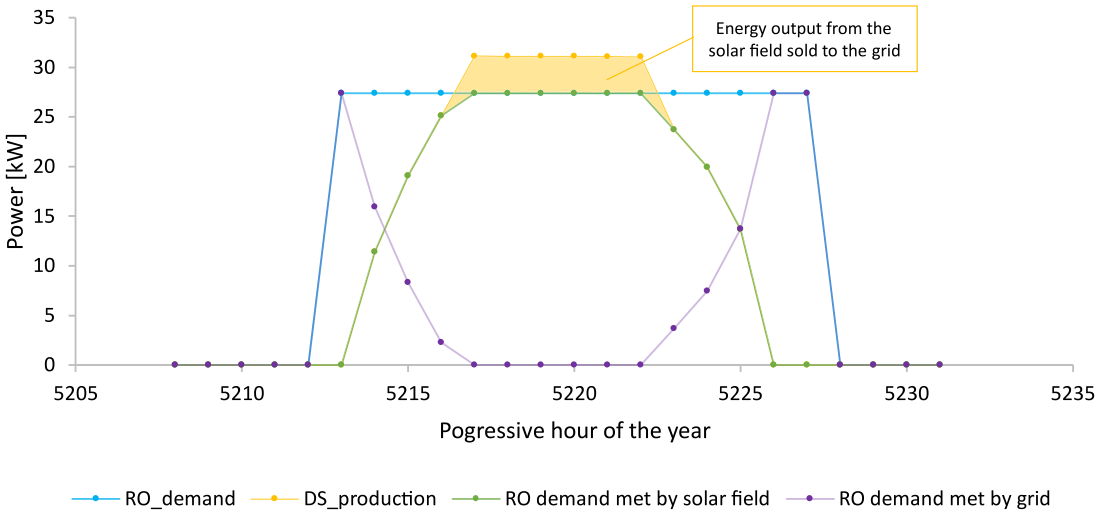

Fig. 13. Output and input power of the examined solar-driven SWRO for a summer day (6th August).. (For interpretation of the references to color in this figure legend, the reader is referred to the web version of this article.)

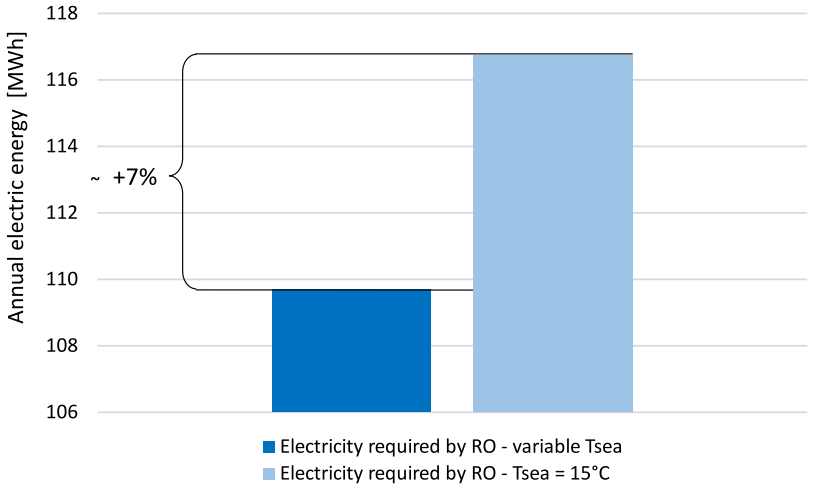

Fig. 14. Electricity required by the RO unit in the case of variable and constant feedwater temperature values.

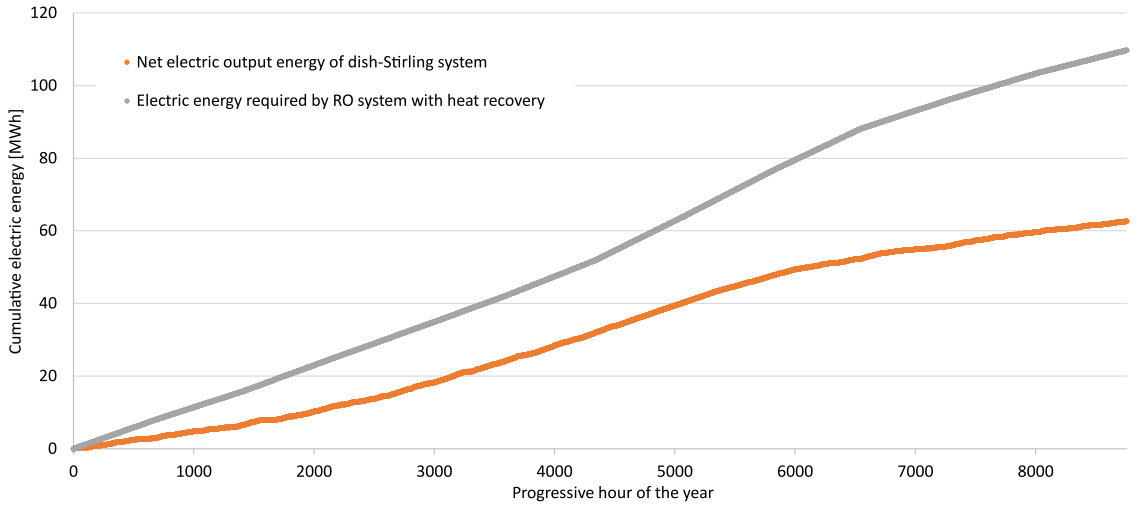

Fig. 15. Annual cumulative curves of the electricity.

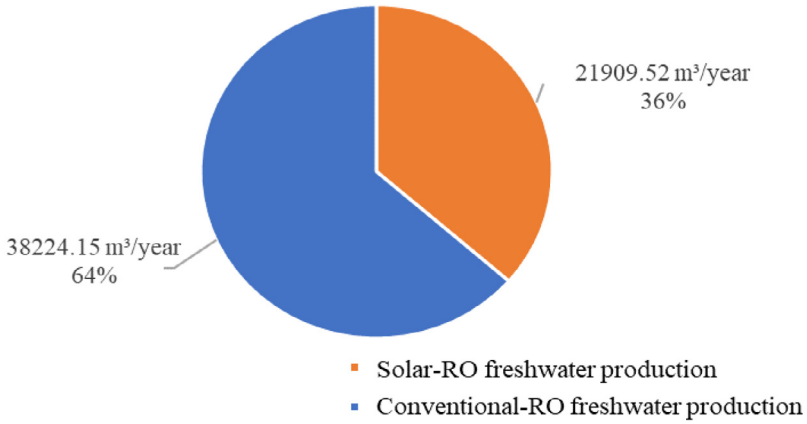

Fig. 16. Fraction of water demand covered by RO system driven by electricity from CSP plant and power grid (with heat recovery).

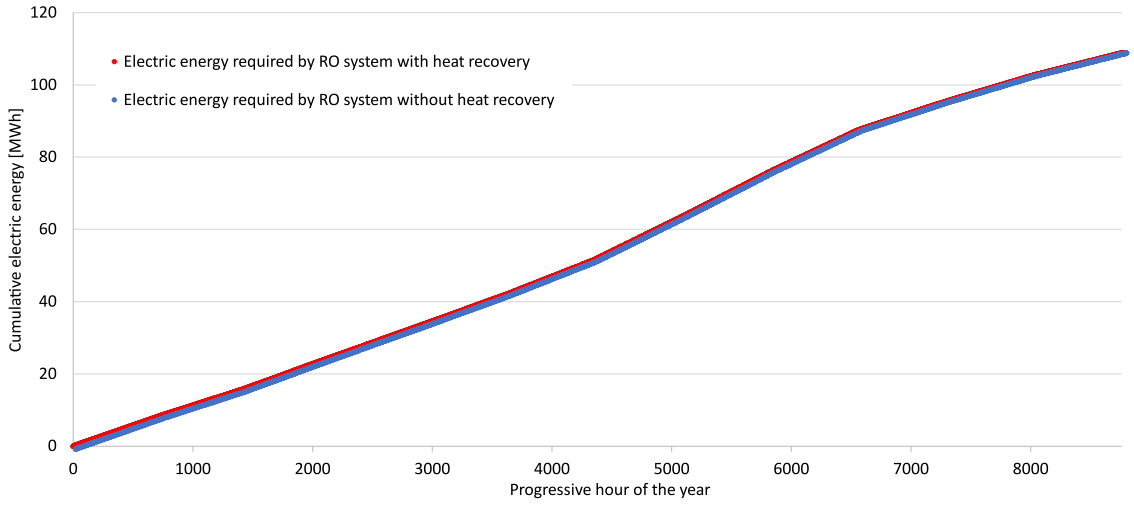

Fig. 17. Annual cumulative curves of electricity required by the RO unit in the presence and absence of heat recovery.

preheating did not lead to a sensible reduction in the energy consumed by the desalination system. More specifically, calculations revealed that this reduction amounts to about 1% and the solar fraction decreases from 0.48 down to 0.47.

4.3. Results of economic and environmental analyses

Under the assumptions defined in Section 3.4, an LCOW value of €1.082/m^3 was obtained for the seawater reverse osmosis desalination plant integrated with a dish-Stirling concentrator. This value appears to be consistent with the data reported in the literature (Caldera et al., 2016).

From an environmental point of view, the electricity generated by the dish-Stirling system, which amounts to 62.6 MWh per year, would allow for avoiding the emission of 34.16 tons per year. Worth noting that this environmental indicator accounts only for the operating phase of the system.

5. Conclusions

In this study, a 3-E analysis of an SWRO desalination system coupled with a dish-Stirling solar concentration system was carried out. The analysis investigated the possibility to cover part of the electrical loads of the high-pressure pump and booster pump, which were included in the RO plant, by using the energy generated by a dish-Stirling system operating in "pure electric" and "cogenerative" mode. Indeed, the energy savings resulting from feedwater pre-heating realized by recovering the low-temperature heat discharged on the cold side of the Stirling engine were evaluated. The results of hourly simulations carried out through the model developed in TRNSYS revealed that the energy production of the cogenerative dish-Stirling, which amounted to approximately 62.6 MWh per year (in Lampedusa), would cover 48% of the overall electrical energy consumption of the RO unit. Meantime, about 36% of Lampedusa's water demand could be met using renewable electricity. Finally, these results were compared with those obtained in case of no preheating of the RO feed water. Therefore, it was observed that pre-heating the water led to approximately 1% of energy savings. The economic analysis was conducted using the LCOW methodology, which resulted in a cost of €1.08 per cubic meter of fresh water, consistent with the data reported in the literature. It was also found that, from an environmental perspective, the system would avoid emitting 34.16 tons of CO_2 equivalent emissions per year. Overall, these results demonstrated the potential benefits of integrating renewable energy sources with desalination systems for sustainable water production in island communities.

NOMENCLATURE

Symbols

a_1	fitting parameter of the linear relationship of Eq. (5) [-]
a_2	fitting parameter of the linear relationship of Eq. (5) [W]
A_{dish}	net effective area of the reflector [m^2]
A_r	aperture area of the receiver [m^2]
c_{energy}	cost related to the purchased electricity [€/kWh]
$C^{RO}_{energy,\,t}$	costs related to the energy purchased from the national grid [€]
$C^{RO}_{M,\,t}$	maintenance costs of the desalination plant [€]
C_t	annual operation cost [€/year]
C^{RO}_t	annual operation cost for the SWRO plant [€/year]
C^{DS}_t	annual operation cost for the dish-Stirling plant [€/year]
$CO_2{}^{av}$	annual amount of avoided CO_2 emissions [tons/year]
$E^{DS}_{exs,\,t}$	annual surplus of energy produced by the solar concentrator and exported to the grid [kWh/year]
$\dot{E}_n$	net electrical output power of the dish-Stirling system [W]
$\dot{E}_p$	electric power absorbed by the parasitic components [W]
$E_r{}^{renew.}$	annual production of electricity from solar energy [kWh/year]
E^{RO}_t	annual energy demand of the SWRO [kWh/year]
f_{sol}	fraction of the energy demand met by solar source [%]
h_r	free convective heat-transfer coefficient at the receiver surface [W/(m^2 K)]
i	discount rate [%]
I_b	solar beam irradiance [W/m^2]
I_0	initial capital investment [€]
I^{RO}_0	capital investment cost for the SWRO plant [€]
I^{DS}_0	capital investment cost for the dish-Stirling plant [€]
$M_{w,t}$	total amount of desalinated water produced in year tth [m^3/year]
n	progressive day of the year [-]
N	lifespan of the plan [years]
p_{ex}	selling price to the grid [€/kWh]
P_f	pressure of feed seawater [bar]
P_p	pressure of permeate water [bar]
$\dot{Q}_{r,in}$	solar input power of the receiver [W]
$\dot{Q}_{r,out}$	thermal output power of the receiver [W]
$\dot{Q}_{solar}$	solar input power collected by the paraboloidal reflector [W]
$\dot{Q}_{S,in}$	high-temperature thermal power delivered to the Stirling engine [W]
$\dot{Q}_{S,out}$	low-temperature thermal power discharged from the cold side of the Stirling engine [W]
R	permeate recovery ratio [-]
R_t	revenue resulting from the sale of surplus electricity produced by the solar concentrator [€/year]
R_T	air temperature correction factor [-]
SEC	Specific Energy Consumption [kWh/m^3]
T_{air}	external air temperature [°C]
T_f	feed water temperature [°C]
T_{sea}	seawater temperature [°C]
T^{ave}_r	average value of the receiver surface temperature [°C]
T_{sky}	the effective sky temperature [°C]
$\dot{V}_p$	permeate water flow rate [m^3/h]
W_S	mechanical power produced by the Stirling engine [W]
W_{tot}	total power required by the hydraulic pumps [kW]

Greek letters

α	absorbance of the receiver cavity [-]
β	leakage water flow rate fraction [-]
γ	intercept factor [-]
ΔP	pressure difference across the reverse osmosis unit [bar]
ε	emissivity of the receiver surface [-]
η	efficiency of the two pressure pumps in the circuit [-]
η_{cle}	cleanliness index of the mirrors [-]
η_e	energy conversion efficiency of the electric generator [-]
η_E	efficiency of the energy recovery device [-]
η_o	optical efficiency of the concentrator [-]
$\mu^{CO_2}_{\substack{fuel\\mix}}$	median value of lifecycle GHG emissions [kgCO_{2e}/kWh]
ρ	reflectivity of clean mirrors [-]
σ	Stefan–Boltzmann constant [W/(m^2 K^4)]

Abbreviations

BP	Booster Pump
capex	Capital expenditure
CO_2	Carbon Dioxide
CSP	Concentrating Solar Power
ERD	Energy Recovery Device
DNI	Direct Normal Irradiance
GHG	Greenhouse Gas
HEX	Heat EXchanger
HPP	High-Pressure Pump
IEA	International Energy Agency
IRENA	International Renewable Energy Agency
LCOW	Levelized Cost of Water
MED	Multi-Effect Distillation
MSF	Multi-Stage Flash
opex	Operating expenses
PUN	Prezzo Unico Nazionale – purchase cost of electricity
PV	Photovoltaic
PVT	Photovoltaic–Thermal solar collector
RES	Renewable Energy Sources
RO	Reverse Osmosis
SEC	Specific Energy Consumption
SWRO	Seawater Reverse Osmosis
TRNSYS	Transient System Simulation Tool

CRediT authorship contribution statement

S. Guarino: Conceptualization, Methodology, Software, Validation, Investigation, Writing – original draft, Visualization. **P. Catrini:** Conceptualization, Methodology, Investigation, Writing – original draft, Visualization. **A. Buscemi:** Conceptualization, Methodology, Software, Validation. **V. Lo Brano:** Conceptualization, Methodology, Investigation, Resources, Writing – review &

editing, Supervision. **A. Piacentino:** Conceptualization, Methodology, Investigation, Resources, Writing –review & editing, supervision.

Declaration of competing interest

The authors declare the following financial interests/personal relationships which may be considered as potential competing interests: Valerio Lo Brano reports financial support was provided by Government of Italy Ministry of Education University and Research.

Data availability

No data was used for the research described in the article.

Acknowledgment

This study was developed in the framework of the research activities carried out within the Project "Network 4 Energy Sustainable Transition—NEST", SPOKE 1: SOLAR: PV, CSP & CST. Task 1.5.4–1.5.5 concerning the analytical model for predicting the energy output of the dish-Stirling system.

References

Abdelgaied, M., Abdullah, A.S., Kabeel, A.E., Abosheiasha, H.F., 2022. Assessment of an innovative hybrid system of PVT-driven RO desalination unit integrated with solar dish concentrator as preheating unit. Energy Convers. Manag. 258, 115558. http://dx.doi.org/10.1016/J.ENCONMAN.2022.115558.

Aboelmaaref, M.M., Zayed, M.E., Zhao, J., Li, W., Askalany, A.A., Ahmed, M.Salem., Ali, E.S., 2020. Hybrid solar desalination systems driven by parabolic trough and parabolic dish CSP technologies: Technology categorization, thermodynamic performance and economical assessment. Energy Convers. Manag 220, 113103. http://dx.doi.org/10.1016/j.enconman.2020.113103.

Ahmadi, M.H., 2012. Investigation of solar collector design parameters effect onto solar stirling engine efficiency. J. Appl. Mech. Eng. 01, 10–13. http://dx.doi.org/10.4172/2168-9873.1000102.

Al-Dafaie, A.M.A., Dahdolan, M.E., Al-Nimr, M.A., 2016. Utilizing the heat rejected from a solar dish stirling engine in potable water production. Sol. Energy 136, 317–326. http://dx.doi.org/10.1016/j.solener.2016.07.007.

Al-Karaghouli, A., Kazmerski, L.L., 2013. Energy consumption and water production cost of conventional and renewable-energy-powered desalination processes. Renew. Sustain. Energy Rev. 24, 343–356. http://dx.doi.org/10.1016/j.rser.2012.12.064.

Almulla, A., Hamad, A., Gadalla, M., 2005. Integrating hybrid systems with existing thermal desalinationplants. Desalination 174, 171–192. http://dx.doi.org/10.1016/J.DESAL.2004.08.041.

Alsarayreh, A.A., Al-Obaidi, M.A., Al-Hroub, A.M., Patel, R., Mujtaba, I.M., 2020. Evaluation and minimisation of energy consumption in a medium-scale reverse osmosis brackish water desalination plant. J. Clean. Prod. 248, 119220. http://dx.doi.org/10.1016/J.JCLEPRO.2019.119220.

Amr Omar, Li, Q., Saldivia, D., Nashed, A., Dang, B. Van, 2022. Solar-driven water treatment: Generation III - low technology readiness. Solar-Driven Water Treat. 20, 1–261. http://dx.doi.org/10.1016/B978-0-323-90991-4.00001-3.

Bădescu, V., 1991. Note concerning the maximal efficiency and the optimal operating temperature of solar converters with or without concentration. Renew. energy 1, 131–135.

Buscemi, A., Guarino, S., Ciulla, G., Lo Brano, V., 2021. A methodology for optimisation of solar dish-stirling systems size, based on the local frequency distribution of direct normal irradiance. Appl. Energy 303, 117681. http://dx.doi.org/10.1016/j.apenergy.2021.117681.

Buscemi, A., Lo Brano, V., Chiaruzzi, C., Ciulla, G., Kalogeri, C., 2020. A validated energy model of a solar dish-stirling system considering the cleanliness of mirrors. Appl. Energy http://dx.doi.org/10.1016/j.apenergy.2019.114378.

Caldera, U., Bogdanov, D., Breyer, C., 2016. Local cost of seawater RO desalination based on solar PV and wind energy: A global estimate. Desalination 385, 207–216.

Caldera, U., Breyer, C., 2017. Learning curve for seawater reverse osmosis desalination plants: Capital cost trend of the past, present, and future. Water Resour. Res. 53, 10523–10538. http://dx.doi.org/10.1002/2017WR021402.

Casimiro, S., Ahmedb, M.K.A., Cardosoa, J.P., Mendesa, J.F., 2017. Reverse osmosis powered by Concentrating Solar Power (CSP): A case study for trapani. Sicily. Desalin. Water Treat. 61, 183–195.

Coventry, J., Andraka, C., 2017. Dish systems for CSP. Sol. Energy 152, 140–170. http://dx.doi.org/10.1016/J.SOLENER.2017.02.056.

Edenhofer, O., Madruga, R.P., Sokona, Y., Seyboth, K., Matschoss, P., Kadner, S., Zwickel, T., Eickemeier, P., Hansen, G., Schlömer, S., Stechow, C.von., 2011. Renewable energy sources and climate change mitigation: Special report of the intergovernmental panel on climate change. In: Renewable Energy Sources and Climate Change Mitigation: Special Report of the Intergovernmental Panel on Climate Change. http://dx.doi.org/10.1017/CBO9781139151153.

Eke, J., Yusuf, A., Giwa, A., Sodiq, A., 2020. The global status of desalination: An assessment of current desalination technologies, plants and capacity. Desalination 495, 114633. http://dx.doi.org/10.1016/J.DESAL.2020.114633.

Elazhar, F., Touir, J., Elazhar, M., Belhamidi, S., Harrak, N. El, Zdeg, A., Hafsi, M., Amor, Z., Taky, M., Elmidaoui, A., 2015. Techno-economic comparison of reverse osmosis and nanofiltration in desalination of a moroccan brackish groundwater. Desalin. Water Treat 55, 2471–2477. http://dx.doi.org/10.1080/19443994.2014.959739.

Feria-Díaz, J.J., Correa-Mahecha, F., López-Méndez, J.P., Barrera-Rojas, J., 2021. Recent desalination technologies by hybridization and integration with reverse osmosis: A review. Water 13 (1369).

Fiorenza, G., Sharma, V.K., Braccio, G., 2003. Techno-economic evaluation of a solar powered water desalination plant. Energy Convers. Manag. 44, 2217–2240. http://dx.doi.org/10.1016/S0196-8904(02)00247-9.

Geng, D., Cui, J., Fan, L., 2021. Performance investigation of a reverse osmosis desalination system powered by solar dish-stirling engine. Energy Rep. 7, 3844–3856. http://dx.doi.org/10.1016/j.egyr.2021.06.072.

Ghaffour, N., Lattemann, S., Missimer, T., Ng, K.C., Sinha, S., Amy, G., 2014. Renewable energy-driven innovative energy-efficient desalination technologies. Appl. Energy 136, 1155–1165. http://dx.doi.org/10.1016/J.APENERGY.2014.03.033.

Ghazi, Z.M., Rizvi, S.W.F., Shahid, W.M., Abdulhameed, A.M., Saleem, H., Zaidi, S.J., 2022. An overview of water desalination systems integrated with renewable energy sources. Desalination 542, 116063. http://dx.doi.org/10.1016/J.DESAL.2022.116063.

Gökçek, M., Gökçek, Ö.B., 2016. Technical and economic evaluation of freshwater production from a wind-powered small-scale seawater reverse osmosis system (WP-SWRO). Desalination 381, 47–57. http://dx.doi.org/10.1016/j.desal.2015.12.004.

Goosen, M., Mahmoudi, H., Alyousef, Y., Ghaffour, N., 2023. Solar desalination: A review of recent developments in environmental, regulatory and economic issues. Sol. Compass 5, 100034. http://dx.doi.org/10.1016/J.SOLCOM.2023.100034.

Greenlee, L.F., Lawler, D.F., Freeman, B.D., Marrot, B., Moulin, P., 2009. Reverse osmosis desalination: Water sources, technology, and today's challenges. Water Res. 43, 2317–2348. http://dx.doi.org/10.1016/J.WATRES.2009.03.010.

Guarino, S., Buscemi, A., Messineo, A., Brano, 2022. Energy and environmental assessment of a hybrid dish-stirling concentrating solar power plant. Sustain. 14, http://dx.doi.org/10.3390/su14106098.

Guarino, S., Catrini, P., Buscemi, A., Brano, V.Lo., Piacentino, A., 2021. Assessing the energy-saving potential of a dish-stirling con-centrator integrated into energy plants in the tertiary sector. Energies 14, http://dx.doi.org/10.3390/en14041163.

Hondo, H., 2005. Life cycle GHG emission analysis of power generation systems: Japanese case. Energy 30, 2042–2056.

IEA, 2023. Italy, IEA, Paris https://www.iea.org/reports/italy-2023, License: CC BY 4.0.

Karabelas, A.J., Koutsou, C.P., Kostoglou, M., Sioutopoulos, D.C., 2018. Analysis of specific energy consumption in reverse osmosis desalination processes. Desalination 431, 15–21. http://dx.doi.org/10.1016/J.DESAL.2017.04.006.

Kelley, L.C., Dubowsky, S., 2013. Thermal control to maximize photovoltaic powered reverse osmosis desalination systems productivity. Desalination 314, 10–19. http://dx.doi.org/10.1016/J.DESAL.2012.11.036.

Kim, J., Park, K., Yang, D.R., Hong, S., 2019. A comprehensive review of energy consumption of seawater reverse osmosis desalination plants. Appl. Energy 254, 113652. http://dx.doi.org/10.1016/J.APENERGY.2019.113652.

Kongtragool, B., Wongwises, S., 2005. Optimum absorber temperature of a once-reflecting full conical concentrator of a low temperature differential stirling engine. Renew. Energy 30, 1671–1687. http://dx.doi.org/10.1016/j.renene.2005.01.003.

Koutsou, C.P., Kritikos, E., Karabelas, A.J., Kostoglou, M., 2020. Analysis of temperature effects on the specific energy consumption in reverse osmosis

desalination processes. Desalination 476, 114213. http://dx.doi.org/10.1016/j.desal.2019.114213.
Lee, S., Cho, H.-Y., Har, D., 2018. Operation optimization with jointly controlled modules powered by hybrid energy source: A case study of desalination. Renew. Sustain. Energy Rev 81, 3070–3080.
Leijon, J., Forslund, J., Thomas, K., Boström, C., 2018. Marine current energy converters to power a reverse osmosis desalination plant. Energies 11, http://dx.doi.org/10.3390/en11112880.
Li, C., Besarati, S., Goswami, Y., Stefanakos, E., Chen, H., 2013. Reverse osmosis desalination driven by low temperature supercritical organic rankine cycle. Appl. Energy 102, 1071–1080. http://dx.doi.org/10.1016/j.apenergy.2012.06.028.
Lo Brano, V., Guarino, S., Buscemi, A., Bonomolo, M., 2022. Development of neural network prediction models for the energy producibility of a parabolic dish: A comparison with the analytical approach. Energies 15, http://dx.doi.org/10.3390/en15249298.
Loutatidou, S., Arafat, H.A., 2015. Techno-economic analysis of MED and RO desalination powered by low-enthalpy geothermal energy. Desalination 365, 277–292. http://dx.doi.org/10.1016/J.DESAL.2015.03.010.
Nassrullah, H., Anis, S.F., Hashaikeh, R., Hilal, N., 2020. Energy for desalination: A state-of-the-art review. Desalination 491, 114569. http://dx.doi.org/10.1016/J.DESAL.2020.114569.
Okampo, E.J., Nwulu, N., 2021. Optimisation of renewable energy powered reverse osmosis desalination systems: A state-of-the-art review. Renew. Sustain. Energy Rev. 140, 110712. http://dx.doi.org/10.1016/J.RSER.2021.110712.
Palenzuela, P., Ortega-Delgado, B., Alarcón-Padilla, D.-C., 2020. Comparative assessment of the annual electricity and water production by concentrating solar power and desalination plants: A case study. Appl. Therm. Eng. 177, 115485.
Papapetrou, M., Cipollina, A., Commare, U.La., Micale, G., Zaragoza, G., Kosmadakis, G., 2017. Assessment of methodologies and data used to calculate desalination costs. Desalination 419, 8–19. http://dx.doi.org/10.1016/J.DESAL.2017.05.038.
Pfeifroth, U., Kothe, S., Trentmann, J., Hollmann, R., Fuchs, P., Kaiser, J., Werscheck, M., 2019. Surface Radiation Data Set - Heliosat (SARAH) - edition 2.1. Satell. Appl. Facil. Clim. Monit http://dx.doi.org/10.5676/EUM_SAF_CM/SARAH/V002_01.
Sassi, K.M., Mujtaba, I.M., 2013. Optimal operation of RO system with daily variation of freshwater demand and seawater temperature. Comput. Chem. Eng. 59, 101–110. http://dx.doi.org/10.1016/J.COMPCHEMENG.2013.03.020.
Sayyad, S.U., Kamthe, N.K., Sarvade, S.M., 2022. Design and simulation of reverse osmosis process in a hybrid forward osmosis-reverse osmosis system. Chem. Eng. Res. Des. 183, 210–220. http://dx.doi.org/10.1016/J.CHERD.2022.05.002.
Shalaby, S.M., 2017. Reverse osmosis desalination powered by photovoltaic and solar rankine cycle power systems: A review. Renew. Sustain. Energy Rev. 73, 789–797. http://dx.doi.org/10.1016/J.RSER.2017.01.170.
Shalaby, S.M., Sharshir, S.W., Kabeel, A.E., Kandeal, A.W., Abosheiasha, H.F., Abdelgaied, M., Hamed, M.H., Yang, N., 2022. Reverse osmosis desalination systems powered by solar energy: Preheating techniques and brine disposal challenges – A detailed review. Energy Convers. Manag. 251, 114971. http://dx.doi.org/10.1016/j.enconman.2021.114971.
Shenvi, S.S., Isloor, A.M., Ismail, A.F., 2015. A review on RO membrane technology: Developments and challenges. Desalination 368, 10–26. http://dx.doi.org/10.1016/J.DESAL.2014.12.042.
Unfried, K., Kis-Katos, K., Poser, T., 2022. Water scarcity and social conflict. J. Environ. Econ. Manage 113, 102633. http://dx.doi.org/10.1016/J.JEEM.2022.102633.
Weather stats: forecast, statistics, analysis, 2022. [WWW Document], URL https://weather-stats.com/italy/lampedusa/sea_temperature. (Accessed 5 February 2022).
Xevgenos, D., Moustakas, K., Malamis, D., Loizidou, M., 2016. An overview on desalination & sustainability: Renewable energy-driven desalination and brine management. Desalin. Water Treat. 57, 2304–2314. http://dx.doi.org/10.1080/19443994.2014.984927.
Zapata-Sierra, A., Cascajares, M., Alcayde, A., Manzano-Agugliaro, F., 2021. Worldwide research trends on desalination. Desalination 519, 115305. http://dx.doi.org/10.1016/J.DESAL.2021.115305.